Bond behaviour of substandard splices in RC beams externally confined with CFRP

Reyes Garcia[a*], Yasser Helal[a], Kypros Pilakoutas[a], Maurizio Guadagnini[a]

[a] Dept. of Civil and Structural Engineering, The University of Sheffield, Sir Frederick Mappin Building, Mappin Street, Sheffield, S1 3JD, UK.

Tel.: +44 (0) 114 222 5071. Fax: +44 (0) 114 222 5700

Email (corresponding author*): r.garcia@sheffield.ac.uk

Abstract

Bond splitting is investigated using flexural tests on twelve RC beams with substandard laps (25 bar diameters) at midspan. Different confinement configurations of the splice region, concrete covers and bar sizes are examined. The results show that CFRP confinement enhances the splice bond strength by up to 65% compared to unconfined specimens. Predictive equations from the literature are shown to yield a large scatter in results and to overestimate the strain developed in the CFRP confinement. An alternative approach to calculate the confinement strain and the additional bond strength provided by CFRP confinement is proposed and validated.

Keywords: substandard lap splices; seismic strengthening; RC beams; CFRP confinement; bond-splitting strength; bar slip

1 Introduction

Disastrous human and economic losses in recent destructive earthquakes (Kashmir, 2005; China, 2008; Indonesia and Italy, 2009; Haiti, 2010) are a consequence of the high seismic vulnerability of existing substandard buildings, a large proportion of which is reinforced concrete (RC). Many catastrophic failures in RC structures can be attributed to failure of inadequate spliced reinforcement at locations of large demand, such as column-footing interfaces or in starter bars above beam-column joints. The local strengthening of these deficient members is a feasible option for reducing the seismic vulnerability of such substandard buildings. Over the last two decades, externally bonded fibre reinforced polymers (FRP) have been used widely to strengthen seismically deficient members. Compared to other strengthening materials, FRP possess advantages such as high strength to weight ratio, high resistance to corrosion, excellent durability, ease and speed of in-situ application and flexibility to strengthen selectively only those members seismically deficient [1].

Many experimental studies have shown the effectiveness of FRP confinement at improving the behaviour of columns with inadequate short lapped reinforcement (e.g. lap length l_b=20-35d_b, where d_b is the bar size) [2-15]. Despite the extensive research efforts, relatively little research has focused on developing appropriate analytical models for the strengthening of column splices using FRP materials. Seible et al. [4] proposed the first model for FRP strengthening of short lapped bars in columns where failure was governed by splitting. Whilst this model is included in current FRP guidelines [16-17], its use in actual strengthening applications may lead to very conservative amounts of FRP confinement [7,11].

More recently, the strengthening of short laps with FRP materials was investigated by adopting a bond approach similar to that used for internal steel stirrups [13,18,19]. The results of these studies indicate that a) the maximum bond strength of the lapped bars could be developed using less confinement than that recommended by current FRP strengthening guidelines, and b) in splitting-prone RC members, FRP confinement is effective at enhancing bond strength up to the point where bar pullout dominates failure. Based on limited experimental work, some analytical models were proposed to compute the additional contribution of FRP confinement to the bond strength of splices [e.g. 13,18,19]. These models are mainly based on modifications of existing equations originally developed for steel confinement, and assume the

total bond strength of a lap as the sum of the individual contributions of concrete cover and FRP confinement. Therefore, the concrete contribution to bond strength is computed using bond strength equations available in the literature, whereas the contribution of the FRP confinement is computed by adopting either i) a "strain approach" that considers the effective strain developed in the FRP [e.g 13,18], or ii) an equivalent area of FRP confinement accounting for the different stiffness of steel stirrups and FRP [19]. Recent research by the authors on very short splices [20] showed that these models overestimate the strains developed in carbon FRP (CFRP) confinement and show a large scatter when predicting experimental results. Based on results from twelve CFRP-confined short beams with very short splices (l_b=10d_b), a new strain approach was proposed that yields more consistent predictions of bond strength enhancement due to FRP confinement. However, the accuracy of the proposed approach needs to be verified using tests on lap splices as those found in typical substandard RC constructions.

This research is part of a multistage research project focusing on the seismic strengthening of substandard RC buildings [20-25]. This paper investigates the effectiveness of externally bonded carbon FRP (CFRP) confinement at enhancing the bond strength of substandard lapped bars (l_b=25d_b) in RC beams. The test results are used to examine and discuss the accuracy of predictive models available in the literature.

2 Experimental programme

Twelve RC beams were tested in flexure. The beams were designed to fail by bond-splitting at midspan, where the main bottom reinforcement was lapped. Consequently, the use of confinement at this zone is expected to improve considerably the bond behaviour of the bars.

2.1 Characteristics of beam specimens

The twelve tested beams are "splice specimens" as defined by ACI 408R-03 [26]. The beams had a rectangular cross section of 150×250 mm, a total length of 2500 mm and a clear span of 2300 mm (see Fig. 1a-b). The main flexural reinforcement was lapped at midspan and consisted of two steel bars of diameter d_b=12 or 16 mm. The top beam reinforcement consisted of two continuous 10 mm bars. To prevent shear failure, 8 mm deformed stirrups were placed at 150 mm centres outside the lap splice zone. The lap length selected for the beams (l_b=25d_b) is representative of typical deficient laps of substandard (pre-seismic) RC structures in developing countries. To investigate different concrete cover to diameter

ratios (c/d_b), side and bottom covers of 10 and 20 mm were selected for the beams reinforced with 12 mm bars, whereas 27 mm covers were used for the beams reinforced with 16 mm bars. Different levels of confinement were investigated. Internal steel stirrups were used to confine the splice region of three of the tested beams. To replicate substandard construction detailing, the stirrups were closed with 90° hooks instead of 135° hooks typically required by current seismic codes. CFRP sheets were used for six beams: the midspan of three beams was confined with 1 layer of CFRP confinement and another three with 2 layers. For comparison, three unconfined control beams with lapped bars were also cast.

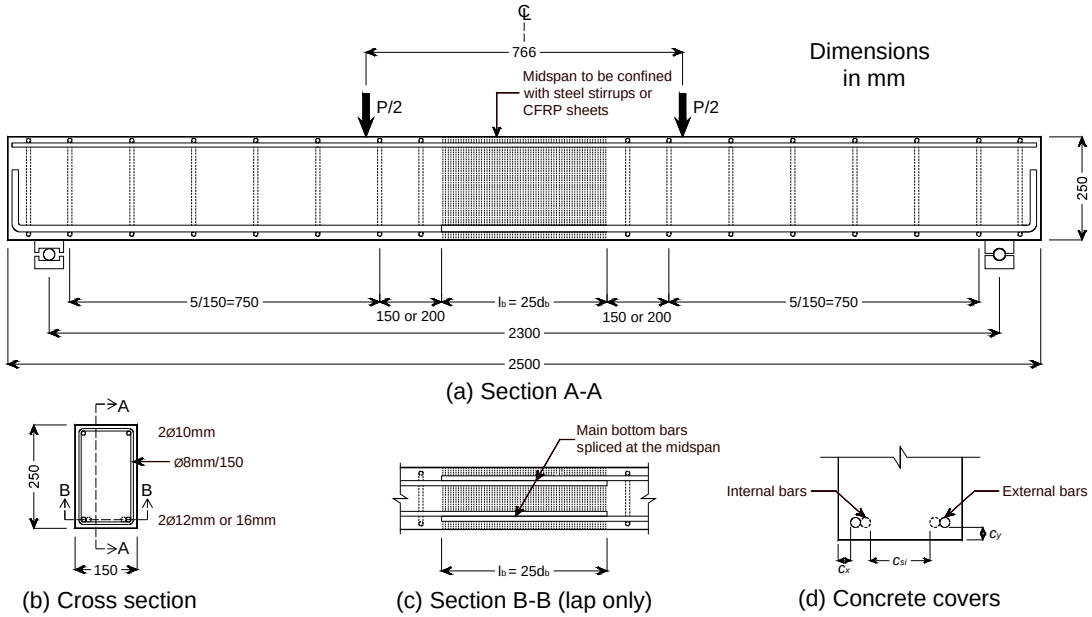

Fig. 1. General geometry and reinforcement details of tested beams.

The main characteristics of the tested beams are shown in Table 1. Beams are identified according to the intended concrete cover c (LC10, LC20 and LC27 for c=10, 20 and 27 mm, respectively) and type of confinement (Ctrl=unconfined control, S=steel-confined, and F=CFRP-confined beams). The last digit of the CFRP-confined beams indicates the number of layers utilised at midspan (1 or 2). Table 1 also reports the measured side (c_x), bottom (c_y) and internal (c_{si}) concrete covers (see definitions in Fig. 1d). These produced c_{min}/d_b ratios ranging from 0.83 to 1.67, where c_{min}=min(c_x, c_y, c_{si}/2).

Table 1. Main characteristics of tested beams

Group	ID	f_{cm} (MPa)	Measured covers (mm)				c_{min}/d_b	Flexural bars	Confinement at midspan
			c_x		c_y	c_{si}			
			Face A	Face B					
LC10	LC10Ctrl	27.9	12	13	11	79	0.92	2Ø12	None
	LC10S	27.9	11	16	13	81	0.92	2Ø12	3Ø8/90 mm
	LC10F1	27.9	15	10	12	81	0.83	2Ø12	1 layer CFRP
	LC10F2	27.9	16	15	11	76	0.92	2Ø12	2 layers CFRP
LC20	LC20Ctrl	24.7	27	22	17	55	1.42	2Ø12	None
	LC20S	24.7	26	21	20	56	1.67	2Ø12	3Ø8/90 mm
	LC20F1	24.7	21	21	17	60	1.42	2Ø12	1 layer CFRP
	LC20F2	24.7	21	20	19	61	1.58	2Ø12	2 layers CFRP
LC27	LC27Ctrl	25.7	25	30	21	31	0.97	2Ø16	None
	LC27S	25.7	30	28	27	29	0.91	2Ø16	3Ø8/90 mm
	LC27F1	25.7	28	28	22	31	0.97	2Ø16	1 layer CFRP
	LC27F2	25.7	28	29	23	28	0.89	2Ø16	2 layers CFRP

2.2 Material properties

Three batches of ready mixed normal-strength concrete were used to cast the beams. The following mix proportions were reported by the supplier: Portland cement CIIIA=125 kg/m^3, GGBS=125 kg/m^3, coarse aggregate 4-10 mm=1002 kg/m^3, sand 0-4 mm=884 kg/m^3, and water/cement ratio=0.8. Casting was performed from the top of the beams so that bars are classified as "bottom cast bars" [26]. After casting, the beams were covered with polythene sheets and wet hessian, cured for seven days in the moulds and subsequently stored under standard laboratory conditions. For each batch, the mean concrete compressive strength (f_{cm}) was obtained from tests on at least three 150×300 mm concrete cylinders according to BS EN 12390-3 [27]. The indirect tensile splitting strength (f_{ctm}) was determined from tests on six 100×200 mm cylinders according to BS EN 12390-6 [28]. The flexural strength (f_{cfm}) was obtained from four-point bending tests on three prisms of 100×100×500 mm according to BS EN 12390-5 [29]. All cylinders and prisms were cast at the same time and cured together with the beams. Table 2 reports the average results and standard deviations for strength from the tests on cylinders and prisms. The elastic modulus of concrete (E_{cm}) was calculated according to Eurocode 2 [30] and the results are also shown in Table 2.

Table 2. Properties of concrete for tested beams

Group	LC10	LC20	LC27
f_{cm} (MPa)	27.9 (1.19)	24.7 (1.06)	25.7 (0.90)
f_{ctm} (MPa)	2.45 (0.24)	2.20 (0.13)	2.48 (0.28)
f_{cfm} (MPa)	3.51 (0.17)	3.54 (0.05)	3.60 (0.09)
E_c (GPa)	29.9	28.9	29.2

Note: standard deviation shown in brackets

The main bottom reinforcement of the beams consisted of high ductility ribbed bars Grade 500 complying with BS 4449:2005 requirements [31]. The mechanical properties of the bars were obtained by testing three bar samples in direct tension. Mean yield and ultimate strength were: f_y=559 and f_u=692 MPa for the 12 mm bar, and f_y=551 and f_u=683 MPa for the 16 mm bar. The elastic modulus of both bars was E_s=209 GPa. Table 3 summarises actual bar rib geometry measurements as provided by the producer.

Table 3. Rib geometry of flexural lap spliced bars

Nominal bar size (mm)		12	16
No. of samples measured		58	245
Rib angle α (°)		35 & 75	35 & 75
Rib inclination β (°)		50	50
Relative rib area (mm^2)	Mean	0.084	0.087
	Std.Dev.	0.006	0.009
Rib height (mm)	Mean	1.02	1.32
	Std.Dev.	0.07	0.08
Average rib spacing (mm)	Mean	7.40	9.42
	Std.Dev.	0.13	0.17

The unidirectional CFRP sheets used as external confinement had the following properties provided by the manufacturer: tensile strength f_f=4140 MPa, modulus of elasticity E_f=241 GPa, ultimate elongation ε_{fu}=1.70%, and thickness sheet t_f=0.185 mm. Before applying the CFRP confinement, concrete surfaces were brushed and cleaned to improve the adherence between the existing concrete and the fibre sheets. Sharp corners within the application zone were rounded off to a radius of 10 mm. The fibres were oriented perpendicular to the beam axis and were applied across the full lap length.

2.3 Test setup and instrumentation

The beams were tested in four-point bending using a 250 kN-capacity servo-controlled actuator and a spreader loading beam as shown in Fig. 2a. This loading arrangement produced a constant moment over the lapped bars at midspan. The beams were simply supported on steel plates and rollers. Linear Variable Displacement Transducers (LVDTs) were used to monitor the vertical deflections of the beams. To measure net deflections, the LVDTs were mounted on an aluminium reference yoke fastened to the beam ends as shown in Fig. 2a. To measure crack opening at the end of the laps, two linear potentiometers with a gauge length of 50 mm were fixed at the level of the spliced bars (see Fig. 2a).

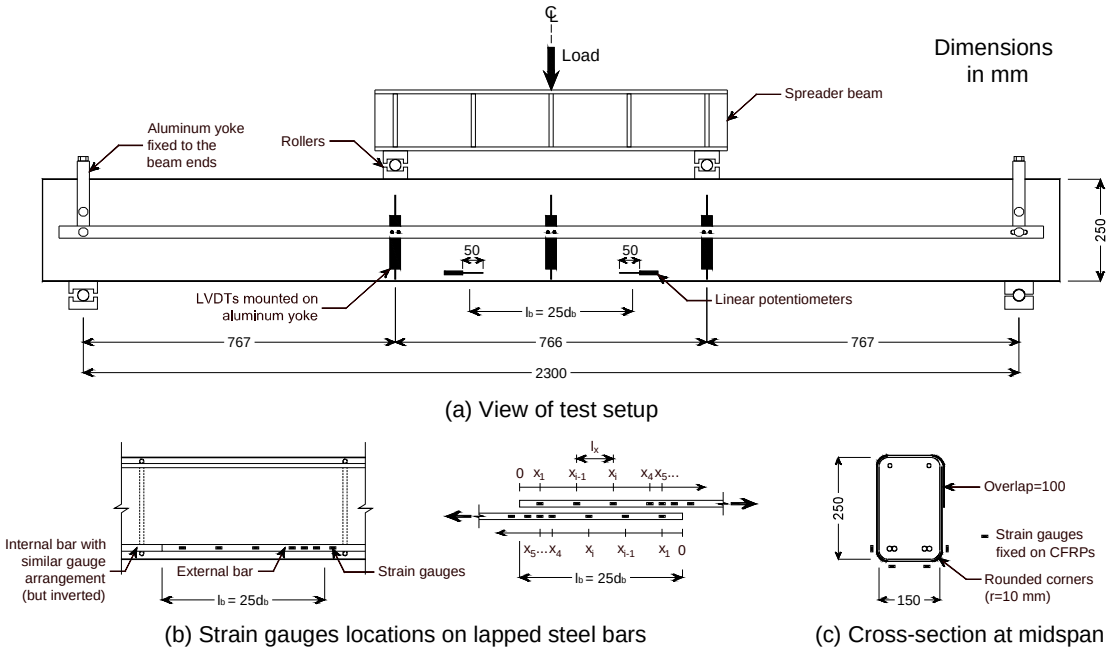

Fig. 2. Test setup and instrumentation of beams.

One of the splices was instrumented with two series of seven 10 mm strain gauges located along the lapped portion of the bars as shown in Fig. 2b. To produce minimal local disturbance of rib geometry, the gauges were fixed along a longitudinal rib of the bar. Four strain gauges were fixed on the CFRP at the locations where splitting cracks were expected, as shown in Fig. 2c. As sudden failure was expected in some specimens, the tests were video recorded to examine the progression of splitting cracks. All beams were tested after 28 days of casting, and 7 days or more after bonding the CFRP. The tests were performed in displacement control. An initial load cycle of 20 kN was applied to crack the beams in flexure. The load was then restored and subsequently increased up to the maximum beam capacity. After

this point, the confined beams were subjected to three full load-reload cycles. The tests were halted when cover splitting occurred (unconfined beams), or when the load-midspan deflection curve was practically horizontal due to a low residual resistance (confined beams).

3 Test results and discussion

Table 4 reports a) the peak load P_{spl} of the tested beams, b) midspan deflection δ_{spl} at P_{spl}, c) enhancement in load (ΔP_{spl}) and deflection ($\Delta\delta_{spl}$) of the steel and CFRP-confined beams over the control beams, d) maximum bar strain and bar stress at peak load ($\varepsilon_{s,spl}$ and $f_{s,spl}$, respectively), and e) post-peak load and deflection at 15% drop of P_{spl} ($P_{85\%}$ and $\delta_{85\%}$, respectively). The table also presents the ratio of load and deflection of the tested beams to that of equivalent benchmark beams with continuous flexural reinforcement (P_{spl}/P_{bmk} and $\delta_{spl}/\delta_{bmk}$, respectively) tested by Al-Sunna et al. [32] and Duranovic et al. [33]. The following sections summarise the most significant observations of the testing programme and discuss the results listed in Table 4.

Table 4. Load, deflection and bar stress results of tested beams

ID	P_{spl} (kN)	δ_{spl} (mm)	ΔP_{spl} (%)	$\Delta\delta_{spl}$ (%)	$\varepsilon_{s,spl}$[(b)] (με)	$f_{s,spl}$[(b)] (MPa)	$P_{85\%}$ (kN)	$\delta_{85\%}$ (mm)	P_{spl}/P_{bmk} (%)	$\delta_{spl}/\delta_{bmk}$ (%)
BSb	72.3	38.2[(a)]	-	-	$\varepsilon_{s,spl}>\varepsilon_y$	$f_s>f_y$	-	-	100	100
LC10Ctrl	36.2	4.20	-	-	1330	279	-	-	50	11
LC10S	46.1	7.34	+27	+74	1995	418	39.1	9.88	64	19
LC10F1	66.5	12.3	+84	+190	3405	559[(c)]	56.2	16.0	92	32
LC10F2	68.5	17.9	+90	+325	14655	560[(c)]	59.2	21.5	95	47
BSa	71.0	40.7[(a)]	-	-	$\varepsilon_{s,spl}>\varepsilon_y$	$f_s>f_y$	-	-	100	100
LC20Ctrl	39.4	6.09	-	-	1650	346	-	-	55	15
LC20S	35.5	6.49	-10	+7	1505	315	30.2	8.63	50	16
LC20F1	61.4	14.7	+56	+140	2920	559[(c)]	52.2	17.4	86	36
LC20F2	59.2	11.7	+50	+92	3580	559[(c)]	50.3	13.1	83	29
SB3	115.9	36.7[(a)]	-	-	$\varepsilon_{s,spl}>\varepsilon_y$	$f_s>f_y$	-	-	100	100
LC27Ctrl	60.9	6.32	-	-	1860	388	-	-	53	17
LC27S	65.4	7.20	+7	+14	1800	375	56.0	8.00	56	20
LC27F1	83.5	11.3	+37	+80	2540	510	71.0	14.0	72	31
LC27F2	98.3	12.6	+61	+100	2965	551[(c)]	83.6	16.4	85	34

[(a)] Maximum deflection at concrete crushing
[(b)] Maximum of the two instrumented bars
[(c)] The bars developed yielding

3.1 Failure mode

In all beams, first flexural cracks developed at the ends of the splice. The unconfined control beams experienced sudden brittle failure due to splitting of the concrete cover around the lapped bars (see typical failure in Fig. 3a and Video 1 in Supplementary Data - include here link to video LC20Ctrl.mp4), which was accompanied by a loud explosive noise. The use of internal stirrups in the lapped zone did not delay the onset of flexural cracking of the steel-confined beams. However, unlike the unconfined beams, large flexural cracks appeared at the location of internal stirrups. At maximum load, splitting cracks formed along the lapped bars. Towards the end of the tests, some concrete detached due to the combination of cover splitting and wide flexural cracks (see Fig. 3b). As the CFRP sheets were bonded directly onto the concrete surface (see Fig. 3c), the onset of splitting cracking in the CFRP-confined beams was not observed. The CFRP confinement controlled the splitting cracks and prevented concrete cover spalling. Nonetheless, towards the end of the tests, wide flexural cracks formed at the ends of the laps outside the confined zone, as the lapped bars pulled out progressively from the concrete. No evident damage occurred at the CFRP sheets during the tests. However, some local fibre debonding occurred at the location of wide flexural and splitting cracks. It should be mentioned that for beams LC10 and LC20, splitting cracks were first observed along the side and bottom concrete covers. Conversely, for beams LC27, concrete splitting occurred first between the splices, and then along the side and bottom covers. This was due to the small spacing between the lapped bars of the latter beams (c_{si}≈30 mm). Regardless of the confinement used at midspan, the progression of splitting cracks observed in the tested beams coincided with that described by Gambarova et al. [34] (see Fig. 4a-c). Due to higher bar stresses, splitting cracks always started at the end of the lapped bars (see Fig. 4a). This produced complete cover splitting along a given length l_1, partial splitting along a length l_2, and no splitting at the middle zone of the lap (length l_3). When the peak splitting load wass reached, complete splitting propagated rapidly towards the centre of the lap (Fig. 4b). Complete splitting along l_2 led to lap failure (see Fig. 4c).

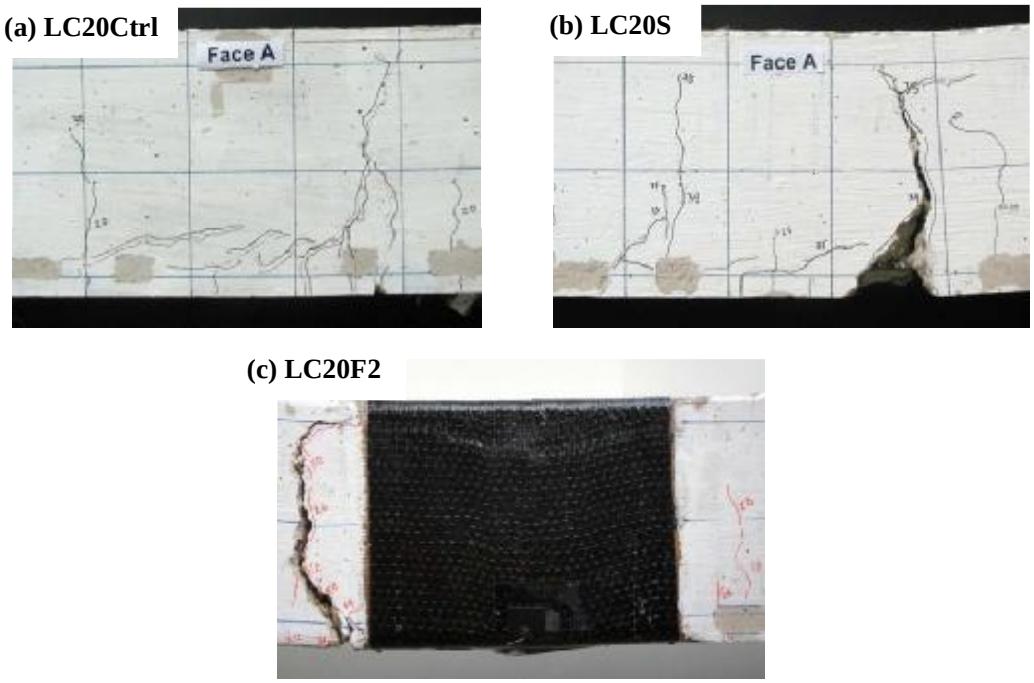

Fig. 3. Typical failures at midspan of beams: (a) unconfined control, (b) steel-confined, and (c) CFRP-confined.

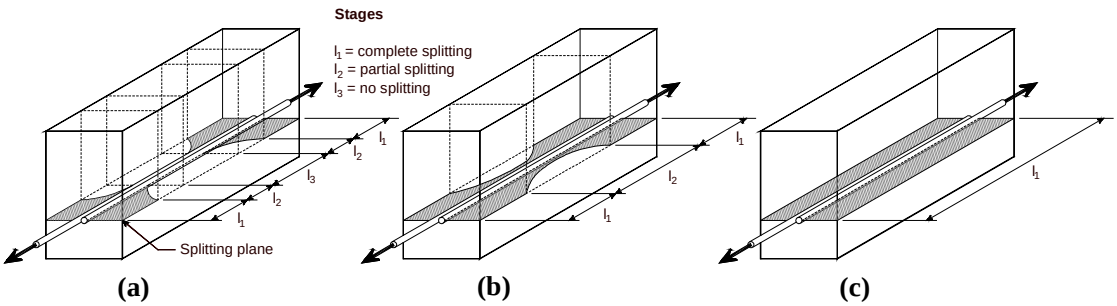

Fig. 4. Typical progression of splitting cracks just before complete cover splitting, adapted from Gambarova et al. [34]**.**

3.2 Load-deflection response

The experimental load-deflection responses are shown in Fig. 5a-c. In the figures, the brittle failure of the unconfined beams is indicated by a star. Comparatively, the use of internal confinement in the lapped zone led to a ductile response, characterised by a gentle drop of the load capacity after the maximum load. The deflections at peak load of the steel-confined beams increased by up to 74% (beam LC10S) when compared to their unconfined counterparts (see Table 4). On the contrary, steel-confined beams only resisted similar or slightly higher loads (by up to 27%) than unconfined beams. The bar stresses shown in Table 4 indicate that the splices of the steel-confined beams remained in the elastic range.

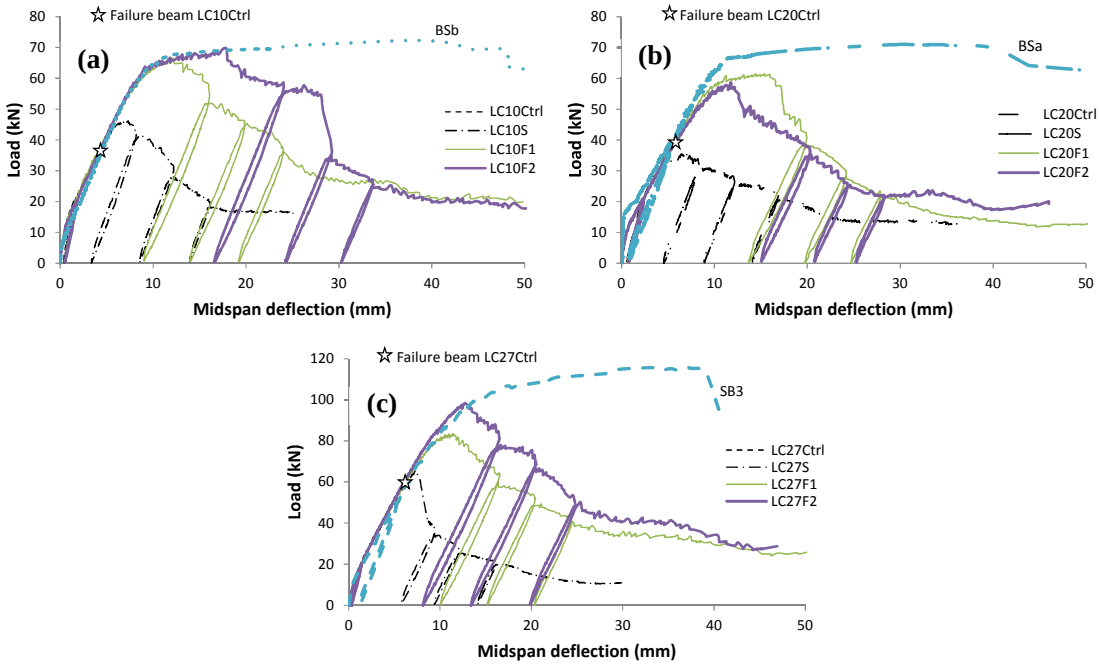

Fig. 5. Load-midspan deflection response of tested beams (a) LC10, (b) LC20, and (c) LC27.

CFRP confinement was very effective at improving the load-deflection behaviour of the beams by delaying the splitting failure. Moreover, with the exception of beam LC27F1, all CFRP-confined beams developed some yielding as indicated by the short post-yield plateaus in Fig. 5a-c (see also $\varepsilon_{s,spl}$ values in Table 4). Maximum loads and deflections were consistently higher compared to their unconfined and steel-confined counterparts. As shown in Table 4, peak loads increased by up to 90% with reference to the unconfined specimens (beam LC10F2). Beams confined with 2 CFRP layers sustained slightly higher loads than those confined with 1 layer (except for beams LC20). The use of CFRP confinement also increased the deflection at peak load by up to 325% (beam LC10F2). Even after a drop of 15% of the peak load, the loads and deflections were up to 73% (beam LC20F1) and 118% (beam LC10F2) higher than those of steel-confined specimens, respectively.

With the exception of beam LC27F1, Fig. 5 and Table 4 show that the CFRP-confined beams resisted similar loads than the corresponding benchmark beams with continuous main bottom bars. The slightly higher capacity of the benchmark beams can be due to the higher yield strength of the reinforcement (f_y=590 MPa) and to some strain hardening at peak load. Overall, the test results indicate that even small amounts of CFRP confinement are sufficient to develop yielding in relatively short splices, which leads to load capacities comparable to those of beams without splices (see ratios P_{spl}/P_{bmk} in Table 4). However,

the ratios $\delta_{spl}/\delta_{bmk}$ in Table 4 (which range from 29% to 49%) also show that splice yielding does not guarantee a fully ductile response of the beams.

3.3 Bond-slip response of spliced bars

The readings from the bar strain gauges are utilised to examine in detail the bond stress and bar slip response of the individual lapped bars. The average bond stress ($\bar{\tau}$) between two strain gauges separated a distance l_x (see Fig. 2c) can be computed using the rate of change of stress (df_s) between them according to Eq. (1) [35,36]:

$$\bar{\tau} = \frac{d_b}{4}\left(\frac{df_s}{l_x}\right) = \frac{d_b}{4}\left(\frac{f_{s,i} - f_{s,i-1}}{x_i - x_{i-1}}\right) \quad (1)$$

where d_b is the bar diameter; x_i and x_{i-1} are the distances to the strain gauges measured from the unloaded end of the bar (l_x=x_i-x_{i-1}, see Fig. 2c); and $f_{s,i}$ and $f_{s,i-1}$ are the bar stresses at distances i and i-1, respectively. The bar stress f_s is computed using the experimental bar strains (ε_s) and a simplified bilinear tensile stress-strain model of steel:

$$f_s = \varepsilon_s E_s \quad \text{for } \varepsilon_s \le \varepsilon_y \quad (2)$$

$$f_s = f_y + (\varepsilon_s - \varepsilon_y)E_{sh} \quad \text{for } \varepsilon_s > \varepsilon_y \quad (3)$$

where E_s and E_{sh} are the elastic and post-yield modulus of steel, respectively, and ε_y is the yield strain of the bar. E_s was taken from the test data of the bars, whilst E_{sh} was assumed to be equal to 0.01E_s to approximately match the direct tension results of the bars (see Fig. 6).

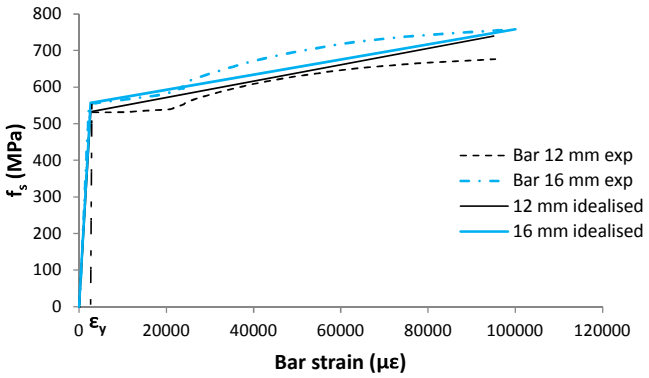

Fig. 6. Idealised stress-strain behaviour of bars and bar test results.

Fig. 7a-d show typical strain and bond stress distributions of the spliced bars of steel and CFRP-confined beams computed using Eqs. (1) to (3). For clarity, the results are presented at load intervals of approximately 10 kN and only up to the peak load. As expected, strains are larger at the loaded end of the bars and reduce progressively towards the unloaded end, where zero strain is assumed. In general, and despite some discrepancies, strain distributions are approximately linear up to the peak load. Whilst the bars of unconfined and steel-confined beams remained elastic, the strain values in Fig. 7c confirm that the bars of CFRP-confined beams developed some yielding.

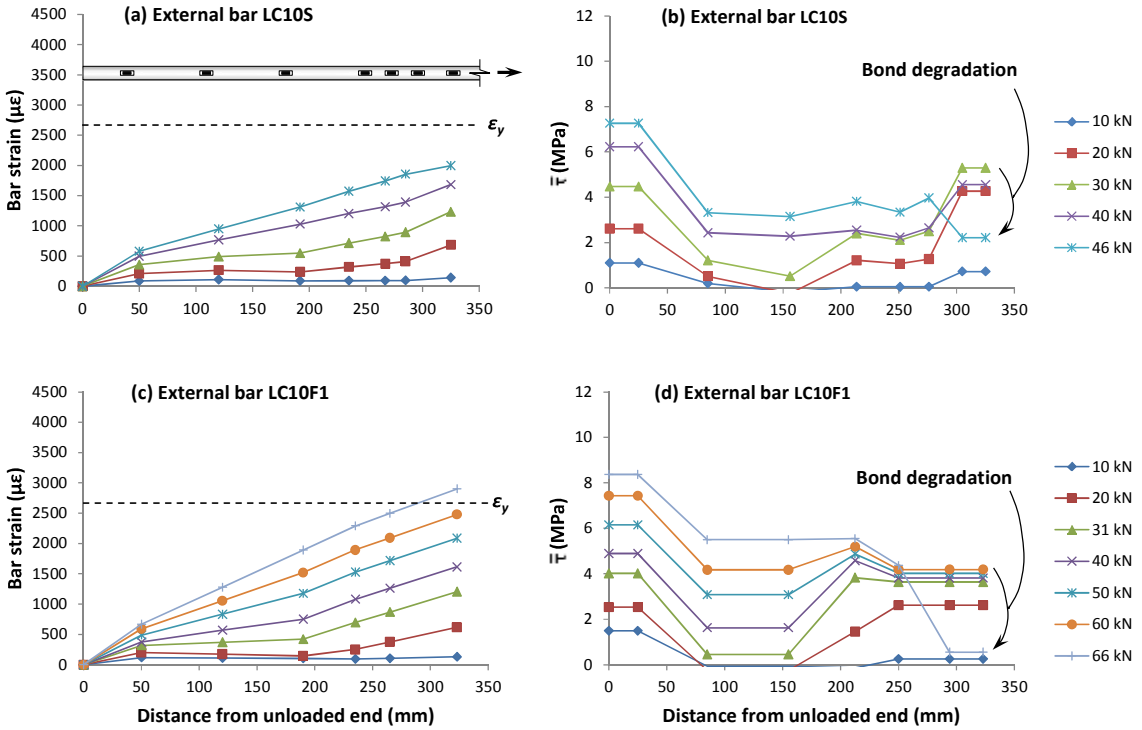

Fig. 7. Typical strain and bond stress distributions of spliced bars in steel and CFRP-confined beams.

Fig. 7b and d show that at the beginning of the tests (P=10 and 20 kN) higher bond stresses developed close to the ends of the lapped bars, whilst low bond stresses were mobilised within the middle zone. As the load increased, the bond stress demand also increased gradually in the middle zone. At peak load, bond stresses were almost uniform along the bar length. The discrepancies in the bond stress profile indicate that flexural cracks also influence the strain distribution. It should be noted that, at peak load, bond stresses at the loaded end of the bars degraded significantly (see loaded ends of Fig. 7b and d). This can be attributed to i) concrete cover splitting around the bars in the case of steel-confined beams, and ii)

bar yielding in the case of CFRP confined beams. This corroborates previous research results [35-37] that indicate that yielding reduces the local bond stress in a similar manner as concrete cover splitting.

In this paper, "bar slip" is defined as the movement of the unloaded end of a bar with reference to its original position. As bar slip at the unloaded end (s_u) was not measured, its value was computed indirectly using crack width measurements from two linear potentiometers located at the bar ends (see Fig. 2a). In addition to s_u, the measured crack widths include slips due to the bar elongation along the splice, s_{el}. Therefore, to obtain s_u, s_{el} was computed using Eq. (4) and then subtracted from the crack width measurements:

$$s_{el,i} = s_{el,i-1} + \frac{1}{2}\left(\frac{\varepsilon_{s,i} + \varepsilon_{s,i-1}}{x_i - x_{i-1}}\right) \quad (4)$$

where $s_{el,i}$ and $s_{el,i\text{-}1}$ are the slips due to bar elongation at distances i and i-1, respectively (see Fig. 2c), and $\varepsilon_{s,i}$ and $\varepsilon_{s,i\text{-}1}$ are the corresponding experimental bar strains. It should be noted that Eq. (4) represents the area of the bar strain distribution along the bars (i.e. Fig. 7a and c) and includes the elastic and inelastic bar elongation.

Fig. 8a-c show the bond-slip responses of the tested beams. For clarity, only the envelope responses are presented. In these figures, bond stress τ is the average stress along the lap length. Fig. 8b-c show the response of some beams only up to the point where the potentiometers failed. It is shown that, during the initial loading, the bond-slip relationships of all beams were similar and negligible bar slips occurred. In the CFRP-confined beams, significant cover splitting occurred at bond stresses of approximately 80-90% the bond strength. After the peak load and for the same slip value, the bond stress sustained by the CFRP-confined beams was consistently higher due to the delay in splitting crack propagation. As can be seen, some bond-slip curves of the CFRP-confined beams exhibit plateaus of relatively constant bond stress. This behaviour can be attributed to the small post-yield steel stiffness assumed in the calculations of bond and to bar pullout. After the bond capacity of the bars was exhausted, bond stress degraded with increasing slip. The results indicate that although CFRP confinement may lead to bar yielding of substandard splices, it may not be sufficient to produce a fully ductile behaviour as bar pullout can govern

failure. In general terms, beams confined with 2 CFRP layers showed a slightly better response than those confined with 1 layer.

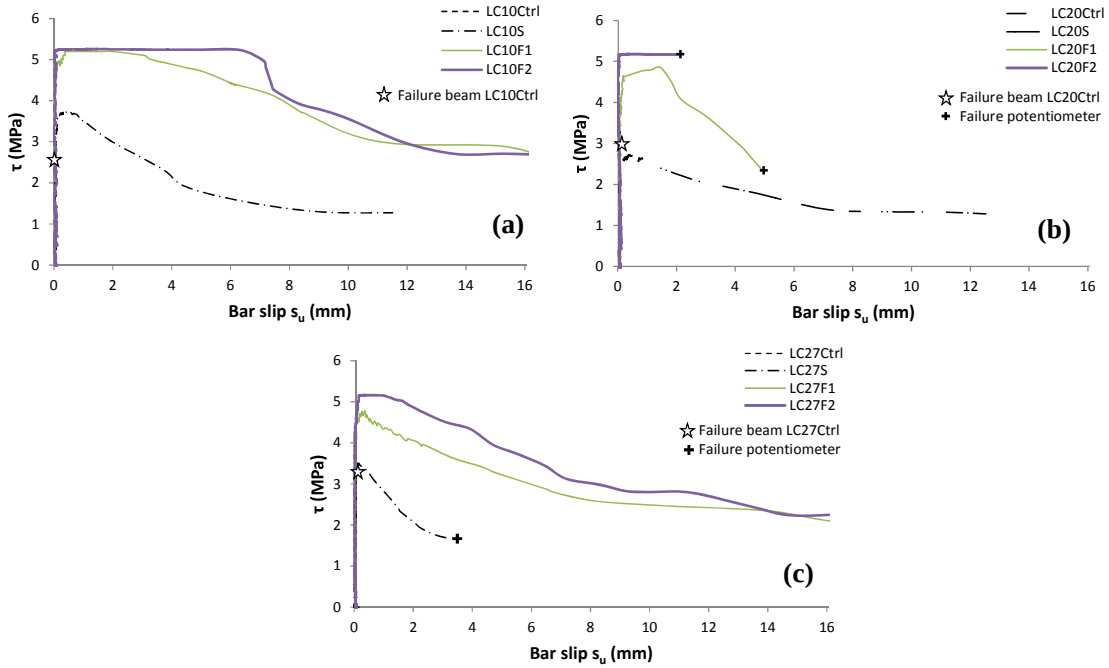

Fig. 8. Bond-slip relationships of tested beams (a) LC10, (b) LC20, and (c) LC27.

It should be mentioned that, compared to its steel-confined counterpart, the experimental bond strength of beam LC10Ctrl was suspiciously low (τ_{spl}=2.50 MPa). A post-failure inspection of this beam revealed that the concrete around the splices had little coarse aggregate, possibly due to the small cover used (minimum cover c_{min}=11 mm). As this lack of aggregate may have led to the premature splitting and failure of this beam, the bond strength of beam LC10Ctrl was computed using the equation proposed by Lettow and Eligehausen [38], which is included (in a simplified form) in Model Code 2010 [39]. This latter value is used in the following analysis and discussions.

Table 5 summarises the results of the tested beams at peak load: a) bond strength τ_{spl}, b) bond strength enhancement due to confinement $\Delta\tau_{spl}$, c) normalised bond strength enhancement $\Delta\tau^{*}_{spl}=\Delta\tau_{spl}/\sqrt{f_{cm}}$, d) bar slip s_u, e) bar slip enhancement due to confinement Δs_u, and f) strain in the CFRP confinement $\varepsilon_{f,spl}$. The value $\Delta\tau_{spl}$ was computed as the difference between the bond strength of the confined beams and that of the corresponding unconfined control beam. The reported CFRP strains are the average readings from the strain gauges shown in Fig. 2c. As shown in Table 5, the premature failure of the unconfined beams is

clearly reflected in the very low bar slip values recorded during the tests (0.012 to 0.041 mm only). Although the bond strength of the steel-confined beams was similar or slightly higher than that of the unconfined beams, the use of steel stirrups enabled the development of a larger bar slip at failure by up to 2790% (beam SC10S). The results also emphasise the effectiveness of CFRP confinement at improving the bond-slip behaviour of the beams. Compared to unconfined specimens, the normalised bond strength was enhanced by up to 57% and 65% for 1 and 2 CFRP confinement layers, respectively (see beams LC10). Moreover, the CFRP confinement increased considerably the slip at peak load by a minimum of 6400% (beam LC10F1) and up to 14000% (beam LC10F2).

Table 5. Bond-slip and CFRP strain results of tested beams

ID	τ_{spl} (MPa)	$\Delta\tau_{spl}$ (MPa)	$\Delta\tau^*_{spl}$ [(b)] ($\sqrt{}$MPa)	$\Delta\tau^*_{spl}$ (%)	s_u (mm)	Δs_u (%)	$\varepsilon_{f,spl}$ (με)
LC10Ctrl	3.31[(a)]	-	-	-	0.012	-	-
LC10S	3.76	0.45	0.08	+14	0.34	+2790	-
LC10F1	5.20	1.89	0.36	+57	0.76	+6400	1570
LC10F2	5.47	2.16	0.41	+65	1.64	+14000	910
LC20Ctrl	3.35	-	-	-	0.027	-	-
LC20S	2.73	-0.62	-0.13	-19	0.31	+1040	-
LC20F1	4.86	1.51	0.30	+45	1.08	+3930	720
LC20F2	5.18	1.83	0.37	+55	0.27	+920	740
LC27Ctrl	3.30	-	-	-	0.041	-	-
LC27S	3.50	0.20	0.04	+6	0.08	+100	-
LC27F1	4.80	1.50	0.30	+45	0.32	+670	1540
LC27F2	5.16	1.86	0.37	+56	0.32	+670	925

[(a)] Original value τ_{spl}=2.50 MPa
[(b)] Bond strength enhancement normalised by $\sqrt{f_{cm}}$

The current test results indicate that 1 or 2 layers of CFRP confinement were sufficient to develop some yielding in the substandard splices of the beams. As the maximum splice bond strength is developed, additional CFRP confinement is not expected to enhance considerably the normalised bond strength in the post-yield stage (as shown by the yielding plateaus in Fig. 8a-c). This is also confirmed in Table 5, where the maximum normalised bond strength enhancement never exceeds $\Delta\tau^*_{spl}$=0.41. As a result, it is uneconomical to provide more confinement than that necessary to develop bar yielding (unless it is required for other strengthening objectives). An upper bound limit of $\Delta\tau^*_{spl}$=0.40, also proposed by

Harajli et al. [19] and corroborated by the authors is a previous study on lap splices [20], is adopted in the analytical model discussed below.

4 Bond strength enhancement in CFRP-confined beams

4.1 Prediction of bond strength

An alternative strain approach to calculate the bond strength enhancement due to FRP confinement was proposed recently by Garcia et al. [20]. The approach considers the total bond strength of a lap as the sum of the individual contributions of concrete cover and FRP confinement. Whilst the concrete cover contribution can be computed using bond equations existing in the literature [e.g. 38,40,41], the effect of the CFRP confinement is considered through an additional confining pressure, f_o. The concrete around the lapped bars is regarded as thick-walled cylinders (similarly to Tepfers [42]) of thickness $c_{min(x,y)}$ as shown in Fig. 9a, where $c_{min(x,y)}$=min(c_x, c_y).

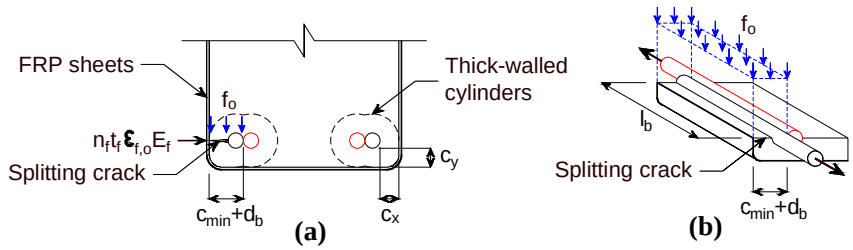

Fig. 9. Bond-splitting failure assumptions in CFRP-confined splices.

The confining pressure f_o is assumed to act over a split cross sectional area equal to $(c_{min(x,y)}+d_b)\cdot l_b$ as shown in Fig. 9b. A strain control approach is adopted to compute f_o, which leads to Eq. (5). The effective CFRP strain $\varepsilon_{f,o}$ is calculated using the concrete tensile strain at the approximate onset of cover splitting, when concrete tensile strains, ε_{ctm}, and CFRP strains are assumed to be equal (perfect bond is assumed). Hence, $\varepsilon_{f,o}=\varepsilon_{ctm}= f_{ctm}/E_{ctm}$, where all the variables were defined previously. f_o is computed as:

$$f_o = \frac{n_f t_f \varepsilon_{f,o} E_f}{n_b (c_{\min(x,y)} + d_b)} \qquad (5)$$

where n_f and t_f are the number of CFRP sheets and thickness of one sheet, respectively; E_f is the elastic modulus of the CFRP; n_b is the total number of pairs of lapped bars in tension, and the rest of the variables are as defined before. It should be mentioned that for discontinuous CFRP applications (strips),

Eq. (5) can be multiplied by w_f/s_f, where w_f and s_f are the width and centre-to-centre spacing of the CFRP strips, respectively. Based on calibration with test data of CFRP-confined beams with very short splices [20], the following relationship between the bond strength enhancement due to CFRP confinement and the confining pressure was found:

$$\Delta\tau^*_{spl} = 1.15\sqrt{f_o} \leq 0.40 \qquad (6)$$

where all the variables are as defined before. In Eq. (6), the maximum normalised bond enhancement is limited to 0.4 as discussed in the previous section.

Table 6 compares the experimental normalised bond strength enhancement ($\Delta\tau^*_{spl}$) with analytical predictions ($\Delta\tau^*_{spl,pred}$) obtained according to Eq. (6) as well as models proposed by Hamad et al. [18], Harajli et al. [19] and Bournas and Triantafillou [13]. The table also summarises the predicted effective CFRP strains ($\varepsilon_{f,pred}$) used for the calculation of $\Delta\tau^*_{spl,pred}$ in Hamad et al. and Bournas and Triantafillou equations. To assess the accuracy of the models, the test/prediction ratios (T/P) and corresponding standard deviations are also reported. Table 6 includes results from beam series S tested by Garcia et al. [20]. Beams S were tested under similar conditions as the current specimens (beams L), but they had different test parameters and a very short lap length of only $10d_b$. Compared to other models, the proposed equation predicts the test results more accurately (mean T/P=1.03) and with less scatter (Std.Dev.=0.08).

Table 6. Test results and analytical predictions of bond strength enhancement, CFRP-confined beams

Beam	$\Delta\tau^*_{spl}$ (√MPa)	Hamad et al. [18]			Harajli et al. [19]		Bournas and Triantifillou [13] [(b)]			Proposed model		
		$\varepsilon_{fe,pred}$ [(a)] (με)	$\Delta\tau^*_{spl,pred}$ (√MPa)	T/P	$\Delta\tau^*_{spl,pred}$ (√MPa)	T/P	$\varepsilon_{fe,pred}$ (με)	$\Delta\tau^*_{spl,pred}$ (√MPa)	T/P	$\varepsilon_{f,o}$ (με)	$\Delta\tau^*_{spl,pred}$ (√MPa)	T/P
SC10F1	0.23	4000	0.25	0.91	0.29	0.78	5950	0.40	0.57	86	0.23	0.97
SC10F2	0.43	4000	0.25	1.72	0.40	1.07	5950	0.40	1.07	94	0.37	1.15
SC20F1	0.22	4000	0.25	0.88	0.29	0.75	5950	0.40	0.55	86	0.22	0.98
SC20F2	0.33	4000	0.25	1.31	0.40	0.82	5950	0.40	0.82	86	0.32	1.03
SC27F1	0.19	4000	0.25	0.74	0.22	0.84	5950	0.26	0.72	86	0.19	0.96
SC27F2	0.25	4000	0.25	1.01	0.40	0.63	5950	0.40	0.63	86	0.27	0.92
LC10F1	0.36	4000	0.25	1.43	0.40	0.90	2650	0.22	1.65	82	0.33	1.08
LC10F2	0.41	4000	0.25	1.63	0.40	1.02	2650	0.40	1.02	82	0.40	1.02
LC20F1	0.30	4000	0.25	1.22	0.40	0.76	2650	0.23	1.33	76	0.28	1.09
LC20F2	0.37	4000	0.25	1.47	0.40	0.92	2650	0.40	0.92	76	0.38	0.97
LC27F1	0.30	4000	0.25	1.18	0.35	0.85	2650	0.15	1.93	85	0.26	1.15
LC27F2	0.37	4000	0.25	1.47	0.40	0.92	2650	0.30	1.22	85	0.36	1.03
Mean				1.25		0.85			1.04			1.03
Std.Dev.				0.31		0.12			0.43			0.08

[(a)] According to ACI 440.2R [43] guidelines for shear strengthening of completely wrapped members

[(b)] Using the modified Lettow and Eligehausen [38] approach proposed by Bournas and Triantifillou [13]

Fig. 10 compares Eq. (6) with the experimental results from beam series S and L. In spite of the different test parameters and lap length examined in these two experimental programmes, it is evident that the proposed equation matches consistently the trend of results. Therefore, it is proposed to use Eqs. (5) and (6) for assessment and strengthening of short splices in substandard RC constructions.

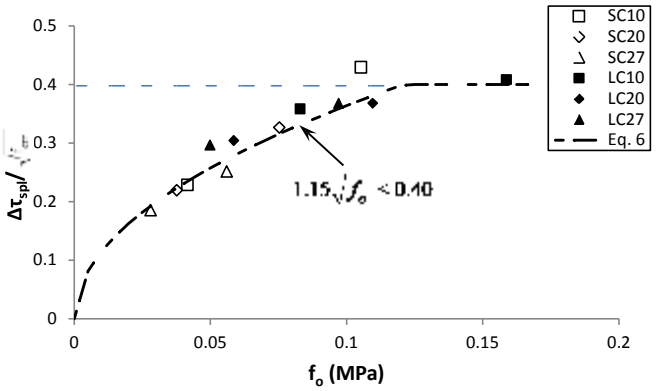

Fig. 10. Comparison of proposed equation with experimental results, CFRP-confined beams.

4.2 Prediction of strains developed in CFRP confinement

To compute the bond strength enhancement due to CFRP confinement, the Hamad et al. [18] and Bournas and Triantafillou [13] models also adopt a "strain approach". For instance, Hamad et al. calculate the effective CFRP strain according to the ACI 440.2R [43] recommendations for shear strengthening. Conversely, Bournas and Triantafillou compute the effective strain as a function of the ratio l_b/d_b. For the beam tested in this research (series L), these two models predict CFRP strain values of 4000 and 2650 με, respectively (see Table 6). However, the current test results show that CFRP strain values never exceeded 1600 με at peak load (see typical results in Fig. 11; see also last column of Table 5). Similar values were reported by the authors for beam series S [20] and by Harajli and Dagher [10]. The results of these experimental studies indicate that Hamad et al. and Bournas and Triantafillou models overpredict considerably the strain values of the CFRP confinement. In addition, Fig. 10 (which shows results of beams with l_b=10 and 25d_b) suggests that the bond strength enhancement due to CFRP confinement is relatively independent of the lap splice length. As a consequence, these results do not support the strain approach proposed by Bournas and Triantafillou.

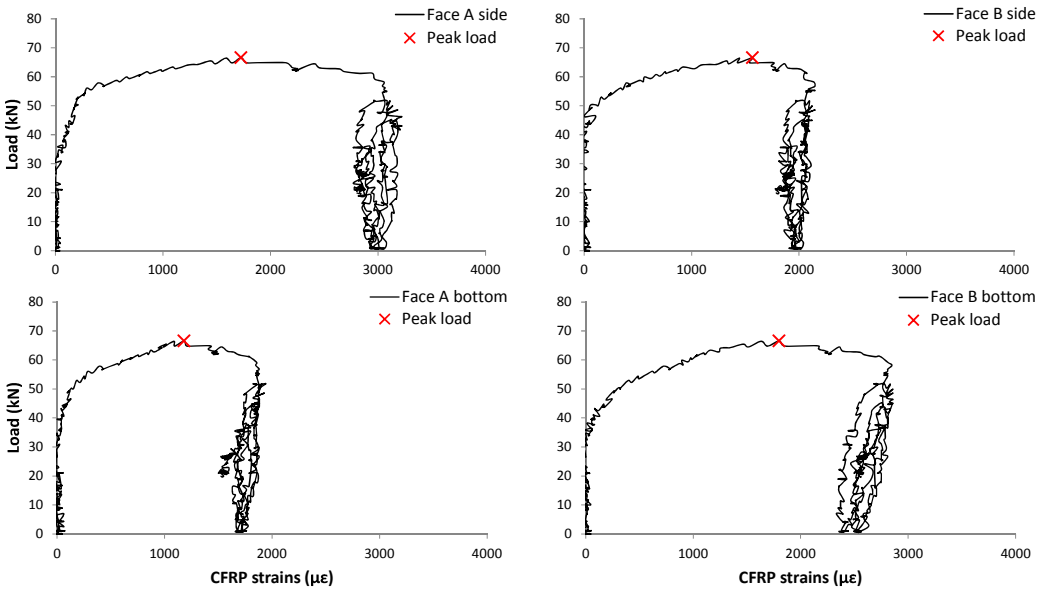

Fig. 11. Typical development of strains in CFRP confinement (beam LC10F1).

As mentioned above, the bond strength enhancement given by Eq. (6) needs to be added to the concrete contribution to compute the total bond strength of the lapped bars, which should be limited to the bond strength at bar yielding. The effectiveness of the proposed model to predict the strength of splices in RC columns confined with CFRP should be further investigated. Until additional experimental data become available, the applicability of the model should be limited to the values $0.8 \leq c_{min(x,y)}/d_b \leq 2.0$. The use of glass, aramid or basalt FRP should be also studied.

5 Conclusions

This study investigated the bond strength enhancement resulting from the confinement provided by externally bonded CFRP in the splice region of RC beams. The beams were subjected to four-point bending and were designed to fail by bond-splitting at midspan, where the main flexural reinforcement was lapped over a length equal to 25 bar diameters. From the analysis and results presented here, the following conclusions can be drawn:

1) The unconfined control beams failed in a brittle manner due to splitting of the concrete cover around the splice. For these beams, bar slip at splitting ranged from 0.012 to 0.041 mm.

2) Compared to unconfined specimens, the use of internal steel stirrups along the splice length resulted in splitting failures at similar or slightly higher loads (by up to 27%) and bond strengths (by up to 14%). However, bar slips increased by up to 2790%. After splitting, the steel-confined beams showed a rather ductile behaviour and sustained significant additional deformations, but with a gradual drop in capacity.

3) The use of externally bonded CFRP confinement delayed the splitting failure of the laps. Compared to unconfined specimens, CFRP confinement also enhanced the bond strength and bar slip by up to 65% and 14000%, respectively. For the beams tested in this study, the use of 1 or 2 CFRP layers was sufficient to develop some yielding in the splice (except for beam LC27F1). The results also indicate that the maximum normalised bond strength enhancement is limited to $\Delta\tau^*_{spl}$=0.40. As no significant bond enhancement is expected in the post-yield stage, it seems uneconomical to provide more confinement than that necessary to develop yielding in the splice.

4) Previous research and the current test results show that splitting failures of laps in CFRP-confined members occur at maximum strain values in the CFRP confinement of 1600 με. This value is considerably lower than the effective CFRP strains predicted by Hamad et al. [18] and Bournas and Triantafillou [13] bond equations (2650-4000 με for the current beams), and supports the new "strain approach" proposed by the authors.

5) Existing equations for predicting the bond strength enhancement due to CFRP confinement show a relatively large variability when compared to experimental results. The new "strain approach" proposed recently by the authors provides more consistent predictions. This can be used for assessment and strengthening of short splices in substandard RC constructions.

Acknowledgements The first author thankfully acknowledges the financial support provided by CONACYT and DGRI-SEP (Mexico). The second author wishes to acknowledge the financial support provided by Damascus University (Syria). The CFRP system was kindly provided by Fyfe Europe S.A.

References

[1] Gdoutos A, Pilakoutas K, Rodopoulos C, editors. Failure analysis of industrial composite materials. 1st ed. New York: McGraw-Hill Companies; 2000.
[2] Saadatmanesh H, Ehsani MR, Jin L. Seismic strengthening of circular bridge pier models with fiber composites. J Struct Eng-ASCE 1996; 91(4):434-47.
[3] Saadatmanesh H, Ehsani MR, Jin L. Seismic retrofitting of rectangular bridge columns with composite straps. Earthq Spectra 1997; 13(2):281-304.

[4] Seible F, Priestley MJN, Hegemier GA, Innamorato D. Seismic retrofit of RC columns with continuous carbon fiber jackets. J Compos Constr 1997; 1(2):52-62.
[5] Ma R, Xiao Y. Seismic retrofit and repair of circular bridge columns with advanced composite materials. Earthq Spectra 1999; 15(4):747-64.
[6] Harajli MH, Rteil AA. Effect of confinement using fiber-reinforced polymer or fiber-reinforced concrete on seismic performance of gravity load-designed columns. ACI Struct J 2004; 101(1):47-56.
[7] Harries KA, Ricles JR, Pessiki S, Sause R. Seismic retrofit of lap splices in nonductile square columns using carbon fiber-reinforced jackets. ACI Struct J 2006; 103(6):874-84.
[8] Bousias S, Spathis A-L, Fardis MN. Seismic retrofitting of columns with lap spliced smooth bars through FRP or concrete jackets. J Earthq Eng 2007; 11(5):653-74.
[9] Breña SF, Schlick BM. Hysteretic behavior of bridge columns with FRP-jacketed lap splices designed for moderate ductility enhancement. J Compos Constr 2007;11(6):565-74.
[10] Harajli MH, Dagher F. Seismic strengthening of bond-critical regions in rectangular reinforced concrete columns using fiber-reinforced polymer wraps. ACI Struct J 2008; 105(1):68-77.
[11] Harajli MH, Khalil Z. Seismic FRP retrofit of bond-critical regions in circular RC columns: Validation of proposed design methods. ACI Struct J 2008; 105(6):760-69.
[12] Elgawady M, Endeshaw M, McLean D, Sack R. Retrofitting of rectangular columns with deficient lap splices. J Compos Constr 2010; 14(1):22-35.
[13] Bournas DA, Triantafillou TC. Bond strength of lap-spliced bars in concrete confined with composite jackets. J Compos Constr 2011; 15(2):156-67.
[14] Elsouri AM, Harajli MH. Seismic repair and strengthening of lap splices in RC columns: carbon fiber-reinforced polymer versus steel confinement. J Compos Constr 2011; 15(5):721-31.
[15] Kim IS, Jirsa JO, Bayrak O. Use of carbon fiber-reinforced polymer anchors to repair and strengthen lap splices of reinforced concrete columns. ACI Struct J 2011; 108(5): 630-40.
[16] CNR-DT 200/2004 Guide for the Design and Construction of Externally Bonded FRP Systems for Strengthening Existing Structures. National Research Council, Rome, Italy; 2004.
[17] BS EN 1998-3 Eurocode 8 - Design of structures for earthquake resistance Part 3: Assessment and retrofitting of buildings. British Standards Institution, London, UK; 2005.
[18] Hamad BS, Rteil AA, Salwan BR, Soudki KA. Behavior of bond-critical regions wrapped with fiber-reinforced polymer sheets in normal and high-strength concrete. J Compos Constr 2004; 8(3):248-57.
[19] Harajli MH, Hamad BS, Rteil AA. Effect of confinement on bond strength between steel bars and concrete. ACI Struct J 2004; 101(5):595-603.
[20] Garcia R, Helal Y, Pilakoutas K, Guadagnini M. Bond strength of short splices in RC beams confined with steel stirrups or external CFRP. Mater Struc 2013; 1-17.
[21] Garcia R, Hajirasouliha I, Pilakoutas K. Seismic behaviour of deficient RC frames strengthened with CFRP composites. Eng Struct 2010; 32(10):3075-85.
[22] Garcia R, Jemaa Y, Helal Y, Pilakoutas K, Guadagnini M. FRP strengthening of seismically deficient full-scale RC beam-column joints. In: Proc. of the 15th World Conf. on Earthq. Eng. 2012. Lisbon, Portugal.
[23] Garcia R, Helal Y, Pilakoutas K, Guadagnini M, Jemaa Y, Hajirasouliha I, Mongabure P. Seismic strengthening of deficient RC buildings using Post-Tensioned Metal Straps: An experimental investigation. In: Proc. of the 15th World Conf. on Earthq. Eng. 2012. Lisbon, Portugal.
[24] Kyriakides N. Vulnerability of RC buildings and risk assessment for Cyprus. PhD Thesis, The University of Sheffield, Sheffield, UK; 2007.
[25] Ahmed S. Seismic vulnerability of non-ductile reinforced concrete structures in developing countries. PhD Thesis, The University of Sheffield, Sheffield, UK; 2011.
[26] ACI 408R-03 - Bond and Development of Straight Reinforcing Bars in Tension. ACI Committee 408, American Concrete Institute, Farmington Hills, Mich.; 2003.
[27] BS EN 12390-3:2009 - Testing hardened concrete Part 3: Compressive strength of test specimens. British Standards Institution, London, UK; 2009a.
[28] BS EN 12390-6:2009 - Testing hardened concrete Part 6: Tensile splitting strength of test specimens. British Standards Institution, London, UK; 2009c.
[29] BS EN 12390-5:2009 - Testing hardened concrete Part 5: Flexural strength of test specimens. British Standards Institution, London, UK; 2009b.
[30] BS EN 1992-1-1 - Eurocode 2: Design of Concrete Structures Part 1-1: General Rules and Rules for Buildings. British Standards Institution, London, UK; 2004.
[31] BS 4449:2005 - Steel for the reinforcement of concrete-Weldable reinforcing steel-Bar, coil and decoiled product-Specification. British Standards Institution, London, UK; 2005.
[32] Al-Sunna R, Pilakoutas K, Hajirasouliha I, Guadagnini M. Deflection behaviour of FRP reinforced concrete beams and slabs: An experimental investigation. Compos Part B-Eng 2012; 43(5):2125-34.
[33] Duranovic N, Pilakoutas K, Waldron P. Tests on Concrete Beams Reinforced with Glass Fibre Reinforced Plastic Bars. In: Proc. of the 3rd Int. Symp. on Non-Metal (FRP) Reinf. for Concr. Struct. 1997. Sapporo, Japan.

[34] Gambarova PO, Rosati GP, Zasso B. Steel-concrete bond after concrete splitting: test results. Mater Struc 1989; 22(1):35-47.
[35] Shima H, Chou L-L, Okamura H. Micro and Macro Models for Bonding Reinforced Concrete. Journal of The Faculty of Engineering, The University of Tokyo (B), Vol. 39 No.2; 1987.
[36] *fib* Bulletin 10 - Bond of reinforcement in concrete. International Federation for Structural Concrete. Laussane, Switzerland; 2000.
[37] Engström B, Magnusson J, Huang Z. Pull-out bond behavior of ribbed bars in normal and high-strength concrete with various confinements. In: Leon R., ed. Bond and development of reinforcement: a tribute to Dr. Peter Gergely. ACI Special Publication 180; 1998.
[38] Lettow S, Eligehausen R. Formulation of application rules for lap splices in the new Model Code. *fib* Task Group 4.5 "Bond models". Stuttgart, Germany; 2006.
[39] *fib* Bulletin 55 - Model Code Volume 1. First complete draft. International Federation for Structural Concrete. Laussane, Switzerland; 2010.
[40] Orangun CO, Jirsa JO, Breen JE. Reevaluation of test data on development length and splices. J Am Concr Inst 1977; 74(3):114-22.
[41] Zuo J, Darwin D. Splice strength of conventional and high relative rib area bars in normal and high-strength concrete. ACI Struct J 2000; 97(4):630-41.
[42] Tepfers R. A theory of bond applied to overlapped tensile reinforcement splices for deformed bars. Publication No. 73:2. Div. of Concr. Struct., Chalmers University of Technology, Goteborg, Sweden; 1973.
[43] ACI 440.2R-08 Guide for the Design and Construction of Externally Bonded FRP Systems for Strengthening Concrete Structures. ACI Committee 440, American Concrete Institute, Farmington Hills, Mich.; 2008.